Gas Giant Magnetosphere-Ionosphere-Thermosphere Coupling

L. C. Ray[1], J. N Yates[2]

[1]Department of Physics, Lancaster University, Lancaster, LA1 4YB
[2]European Space Astronomy Centre (ESAC), European Space Agency, Madrid, Spain

Corresponding author: Licia C. Ray, licia.ray@lancaster.ac.uk

Abstract
Magnetosphere-ionosphere-thermosphere (MIT) coupling describes the exchange of energy and angular momentum between a planet and its surrounding plasma environment. A plethora of phenomena are signatures of this interaction, from bright auroral and radio emissions across multiple wavelengths that are easily observed remotely, to radio bursts and field aligned currents best measured in situ. Gas giant MIT coupling differs from that in the terrestrial system because of rapid planetary rotation rates, dense hydrogen-based atmospheres, and outgassing moons embedded well within the magnetospheres. We discuss here the fundamental physics governing MIT coupling at Jupiter and Saturn.

1 Introduction

Magnetosphere-ionosphere-thermosphere coupling is the process by which energy and angular momentum are transferred between a planet and its surrounding plasma environment. The magnetosphere is host to a variety of plasma populations which are connected to the planetary magnetic field. Stresses associated with changes in magnetic field configuration e.g. magnetic reconnection, magnetospheric compressions or expansions induced by the solar wind, or modifications to the local plasma population e.g. source and/or loss processes such as charge exchange, energisation, plasma injections triggered by reconnection or radial outflow, are communicated to the planet via electrical currents. Electrical currents in the magnetosphere are coupled to the planet through magnetic field-aligned currents which close in the ionosphere. Ionospheric currents modify the coincident thermosphere by for example, heating the local atmosphere and driving winds. Collisions between ionospheric ions and thermospheric neutrals alter the electric currents and thus can affect magnetospheric plasma. Sections 3 and 4 of this series are dedicated to solar wind-magnetosphere and magnetosphere-ionosphere coupling processes, respectively. We concentrate on MIT coupling at the giant planets here.

At Earth, MIT coupling is largely driven by the interaction between the magnetosphere and the solar wind. This is only a fraction of the picture at gas giant planets, where rapid rotation and internal plasma sources combine to drive a more dynamic MIT coupled system. Jupiter and Saturn rotate with periods of $\sim$9.9 hours and $\sim$10.7 hours, respectively. Deep within each magnetosphere, moons under tidal stresses release neutral material into the local space environment. Io ejects $700 - 3000$ kg s^{-1} neutral material into Jupiter's magnetosphere (Delamere, Bagenal, & Steffl, 2005). At Saturn, Enceladus emits neutrals at a rate of $150 - 300$ kg s^{-1} (Hansen et al., 2006). Approximately half of the material remains as plasma in the system following ionization (see Chapter 8.2, this volume).

These plasma sources, embedded well within the magnetosphere, modify the MIT coupling throughout the system from that described in Chapter 4.1. Newly generated plasma, which orbited the planet at the Keplerian velocity as neutrals, must be accelerated to corotation with the planetary magnetic field. This acceleration requires angular momentum to be imparted from the planetary atmosphere to the newly picked-up plasma. Similarly, as plasma is transported radially outwards through the magnetosphere, angular momentum must be transferred from the planet to the magnetospheric plasma to maintain corotation. The MIT coupling driven by these processes is superimposed onto that driven by the solar wind–magnetosphere–ionosphere interaction. The relative contributions of the internal and external MIT coupling drivers shifts with variability in solar wind conditions, moon outgassing rates, and plasma properties such as temperature and composition. In the absence of constellation missions and upstream solar wind monitors, it is difficult to distinguish the timescales and system responses associated with each process. Understanding the observational evidence is critical to provide context for the development of gas giant MIT coupling theory and to test our underlying assumptions and theoretical framework. We focus on non-moon MIT coupling as Section 9 is dedicated to moon-magnetosphere interactions.

1.1 In situ magnetospheric evidence of MIT coupling

In situ and remote observations provide local and global evidence of MIT coupling. In the magnetosphere, indicators of MIT coupling include in situ measurements of the radial angular velocity of corotating plasma (e.g. Bagenal, Wilson, Siler, Paterson, & Kurth, 2016; McNutt, Belcher, Sullivan, Bagenal, & Bridge, 1979; Thomsen et al., 2010), bi-directional electron beams (e.g. Mauk & Saur, 2007; Mitchell et al., 2009), electric currents (e.g. Khurana, 2001), radio emissions (e.g Badman, Cowley, Lamy, Cecconi, & Zarka, 2008; Kurth et al., 2017; Lamy et al., 2018; Zarka, 1998), and measurements of particle acceleration at auroral latitudes (e.g. Allegrini et al., 2017; Clark et al., 2018; Mauk et al., 2017a). Figure 1 shows the plasma flows in the jovian and saturnian magnetospheres as determined from Galileo (Bagenal et al., 2016) and Cassini data (Thomsen et al., 2010). There are large uncertainties in the angular velocities, which depend on both the modeling technique applied and underlying assumptions in the analysis e.g. composition. However, it is clear that the plasma velocity does not have a $r^{-1/2}$ dependence, but instead maintains a near steady rotation rate with respect to corotation. This velocity profile indicates that angular momentum is being extracted from the planet and added to the magnetospheric plasma in order to enforce corotation with the planetary magnetic field.

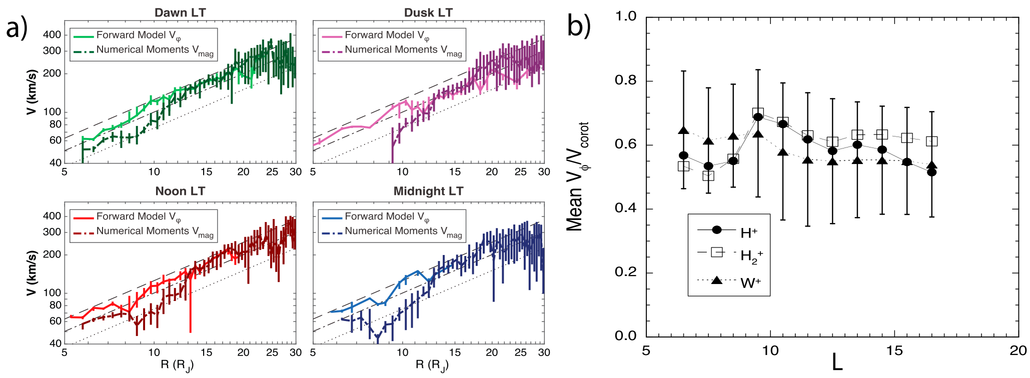

Figure 1. Angular velocities of the magnetospheric plasma at Jupiter and Saturn. a) Galileo azimuthal plasma flows in four local time sectors (adapted from Bagenal et al. (2016)). Dashed, dot-dashed, and dotted lines show 100%, 80%, and 60% of corotation, respectively. b) Azimuthal plasma velocities measured by Cassini at Saturn (adapted from Thomsen et al. (2010)).

Angular momentum is transferred via field-aligned currents, which have also been measured in situ. Mauk and Saur (2007) showed that highly structured field-aligned current systems exist in the jovian magnetosphere. Cassini data at Saturn shows that similar stratification in field-aligned currents exists at high-latitudes that are magnetically connected to the middle and outer magnetosphere (e.g. Hunt et al., 2018; Talboys et al., 2009). Hot electron populations and electron beams have also been measured, which provide a source of current carriers that are able to escape the large potential wells generated by the rapid planetary rotation rate and ensuing ambipolar potentials.

Radio emissions are rife in planetary magnetospheres. These emissions are generated by a host of MIT coupling processes and are a useful diagnostic of the local plasma environment. In the auroral acceleration region, the electron cyclotron maser generates emission (Ergun et al., 2000; Melrose & Dulk, 1982; Wu & Lee, 1979, e.g.). This emission occurs when the plasma frequency is near the local gyrofrequency and hence is a useful diagnostic of both the local plasma conditions and magnetic field structure. Cyclotron maser generated Saturn kilometric radiation is a useful diagnostic of how magnetosphere-ionosphere coupling responds to the solar wind (Badman, Cowley, Gérard, & Grodent, 2006), and plasma injections potential driven by tail reconnection (e.g. Lamy et al., 2013) amongst other processes. At Jupiter, strong decametric radio emissions are invoked by the Io-Jupiter interaction, discussed in Section 9. MIT coupling driven by processes in the middle magnetosphere drives a host of emissions at deca-, hecto-, and kilometer wavelengths (Clarke et al., 2004; Zarka, 1998). Recent Juno observations suggest that source regions for these radio emissions exist throughout the magnetosphere, as the spacecraft passed near 5 source regions alone during the first perijove orbit (Kurth et al., 2017). Furthermore, radio emission that occurs at frequencies below the local electron cyclotron frequency can indicate the presences of Whistler or Alfvén waves, which are important in coupling the magnetosphere and ionosphere (Kurth et al., 2018).

A final piece of magnetospheric evidence is in situ measurements of precipitating particles at high magnetic latitudes. Juno has directly measured precipitating auroral electrons and discovered that mix of acceleration processes occur at Jupiter's magnetosphere (e.g Allegrini et al., 2017; Clark et al., 2018; Mauk et al., 2017a, 2017b). Quasi-static field-aligned potentials, long invoked to be the dominant acceleration process above Jupiter's aurora, are only seen a fraction of the time. Electron intensity profiles instead show that wave-driven stochastic acceleration are prevalent, indicating that MIT coupling at the outer planets is a dynamic, time-dependent process. In both cases, energetic electrons are deposited into the planetary atmosphere generating bright auroral emissions and modifying the underlying ionosphere-thermosphere system.

1.2 Atmospheric evidence of MIT coupling: Auroral observations

Planetary aurorae are the most visual representation of the coupling between a planet's magnetosphere and atmosphere. Earth's aurorae have been observed for thousands of years and have long fascinated humanity. The gas giant planets, Jupiter and Saturn, also have aurorae. Jupiter mainly has auroral emissions in the radio, ultraviolet (UV), infrared (IR) and X-ray wavelengths of the spectrum. Saturn has emissions at the same wavelengths as Jupiter except for X-rays. Both planets have strong radio emissions which have played crucial roles in determining their magnetospheric and rotational properties. Planetary radio emissions are seen as a key way to identify extra solar magnetised planets in the future and are discussed in chapter 11.3. Here, in this chapter, we focus only on auroral emissions from within a planet's upper atmosphere - namely at UV, IR and X-ray wavelengths.

The terrestrial aurora arises due to charged particles travelling along Earth's magnetic field lines colliding with atoms and molecules in the upper atmosphere which in turn emit visible light. It is strongly influenced by the Sun and its magnetic field - permeated throughout the solar system by the solar wind. Gas giant aurora are caused by the same underlying mechanisms as the terrestrial (see chapters 4.1 - 4.5) but in a different parameter space (e.g. higher energies). While the terrestrial aurora is essentially controlled by the solar wind, Jupiter's main auroral oval is controlled predominately by internal sources i.e. the breakdown of corotation of Iogenic plasma slowly diffusing radially outwards. Saturn's aurora appears to be governed by both internal (magnetospheric phenomena) and external (solar wind) sources - a kind of midpoint between the Earth and Jupiter. Jupiter's main oval is ever-present unlike that of the solar system's other magnetised planets, however, both Jupiter's and Saturn's aurora are affected by the solar wind and by transient magnetospheric processes e.g. reconnection. These time-dependent processes result in fine/small-scale auroral features and variations in auroral brightness.

Gas giant aurora is brightest in the UV (100's of kiloRayleighs (kR) at Jupiter and 10's of kR for Saturn) and variations in intensity can be used to diagnose dynamics in the planet's near space environment. Observations of the UV aurora also give information about the energies and fluxes of the precipitating electrons causing the aurorae as well as giving estimates of the temperature of the atmosphere (e.g. Atreya, Donahue, Sandel, Broadfoot, & Smith, 1979). Jupiter's X-ray aurora results from the precipitation of heavy ions into Jupiter's upper atmosphere (e.g. Branduardi-Raymont et al., 2008). The ion species and their energies can give insight into acceleration mechanisms required to energise the ions as well as their region of origin e.g. solar wind for Helium ions or magnetosphere for Sulphur ions (e.g. Dunn et al., 2017). Jupiter's and Saturn's IR aurora results from emission of the H_3^+ ion which is the dominant ion in their ionospheres. IR emission is concurrent in space with UV emission but due to the integration time for each IR observation, short timescale features are often smeared and only large or persistent features are observed. The discovery of H_3^+ emission in gas giant ionospheres (Drossart et al., 1989) allowed for estimates of the temperature of gas giant ionospheres and assuming the atmosphere was in local thermal equilibrium (e.g. Lam et al., 1997; Stallard, Miller, Millward, & Joseph, 2002), one could determine the temperature of the surrounding thermosphere. More recently, H_3^+ emissions have been used to determine the line-of-sight velocity of these ionospheric constituents giving the first remote observations of ionospheric and thermospheric velocities at the gas giant planets (e.g. Johnson, Stallard, Melin, Nichols, & Cowley, 2017; Stallard, Miller, Millward, & Joseph, 2001).

1.3 Models of MIT coupling

There are many different ways to approach MIT coupling. Global magnetospheric dynamics are most often investigated using magneto-hydro-dynamic (MHD) models (e.g. Chané, Saur, Keppens, & Poedts, 2017; Jia, Hansen, et al., 2012; Walker & Ogino, 2003). The inner boundary of these models is a conducting ionosphere, imposed several radii from the planet for computational feasibility. The computational intensity of MHD models prevents a rigorous treatment of the ionosphere yet it is possible to impose ion-neutral collisions (Chané, Saur, & Poedts, 2013) or atmospheric vortices to investigate the feedback between the thermosphere, ionosphere, and magnetosphere (Jia, Kivelson, & Gombosi, 2012). Using these models, it is possible to determine a global view of the MIT coupling currents present in the system. However, it is not possible to include the effects of field-aligned acceleration at high magnetic latitudes, alter the thermospheric velocity due to magnetospheric forcing, or assess the energy balance of the thermosphere using these models.

At the gas giants, quasi-static auroral particle acceleration driven by MIT coupling is explored with Vlasov models that are 1D in space, along the magnetic field, and 2D in velocity space (e.g. Matsuda, Terada, Katoh, & Misawa, 2012; Ray, Galand, Moore, & Fleshman, 2012; Ray, Su, Ergun, Delamere, & Bagenal, 2009; Su, Ergun, Bagenal, & Delamere, 2003). While these models can provide insight into energy intensity profiles of the precipitating auroral particles, plasma density and electric potential structure along the magnetic field, they cannot treat the magnetosphere or ionosphere self-consistently. Instead, Vlasov models use these regions as static boundary conditions. MHD wave-driven and Alfénic acceleration have not yet been modeled outside of moon-magnetosphere interactions at the gas giants (Hess, Delamere, Dols, Bonfond, & Swift, 2010; Hess & Delamere, 2012; Jacobsen, Neubauer, Saur, & Schilling, 2007; Su et al., 2006). However, recent Juno observations show that stochastic acceleration is prevalent within the jovian system and thus future models must consider these effects.

Potentially the most widely used approach in MIT coupling is one-dimensional (1D) models (e.g. Cowley & Bunce, 2001; Hill, 1979; Nichols & Cowley, 2004; D. H. Pontius, 1997; D. H. Pontius & Hill, 2009; D. H. Pontius Jr. & Hill, 1982; Ray, Achilleos, Vogt, & Yates, 2014; Ray, Ergun, Delamere, & Bagenal, 2010; Saur, Mauk, Kaßner, & Neubauer, 2004). Such models investigate radial slices through the system and equate the ionospheric and magnetospheric torques to describe the electric fields, currents, and plasma angular velocities associated with MI coupling. The ionospheric feedback can be explicitly included by modifying the Pedersen conductance with field-aligned current density and electron precipitation energy (Nichols & Cowley, 2004; Ray, Ergun, Delamere, & Bagenal, 2012) and rotational decoupling from field-aligned potentials can be considered (Nichols & Cowley, 2005; Ray et al., 2010). Simplified thermospheric effects are invoked by scaling the Pedersen conductance to account for the subcorotation of the neutral atmosphere due to ion-neutral collisions (D. H. Pontius, 1995).

More detailed MIT coupling models merge the 1D MIT description with a general circulation model of the thermosphere. This approach is optimal for exploring the detailed feedback between the thermosphere, ionosphere, and magnetosphere. Alterations to the thermospheric angular velocity, and their effect on the transfer of angular momentum between the planet and magnetospheric plasma can be explicitly considered. Furthermore, energy inputs into the atmosphere, such as joule heating and ion drag, and their effect on the ionospheric conductance and electric currents are easily quantified (Mueller-Wodarg, 2012; Ray, Achilleos, & Yates, 2015; Smith & Aylward, 2008, 2009; Yates, Achilleos, & Guio, 2012, 2014; Yates, Ray, & Achilleos, 2018). It is this type of model that we consider in this paper. First we discuss the theory behind the magnetosphere-ionosphere coupling portion of the circuit before addressing the physics of the underlying atmosphere.

2 Coupling Theory

Planetary systems are populated by plasma populations under different conditions, from the collisional ionosphere embedded within a planet's thermosphere to collisionless plasma populating the magnetospheric cavity. The planetary magnetic field, which threads all of the plasma, mediates the exchange of angular momentum and energy between the different populations. Electrical currents flow along the magnetic field between the ionosphere and magnetosphere. Within the two regions, currents flow perpendicular to the field with associated $\mathbf{J}\times\mathbf{B}$ forces acting on the local plasma populations.

2.1 One-dimensional approach

Hill (1979) was the first to describe the torque balance between the magnetospheric and ionospheric plasma populations in such systems under the assumptions of a spin-aligned dipole magnetic field, azimuthal symmetry, steady-state transport, constant ionospheric Pedersen conductance, no thermospheric feedback, and equipotential field lines. Mass-loading was later included by D. H. Pontius Jr. and Hill (1982). Numerical descriptions followed in the early 2000s, which explored how the MIT coupling changes as these simplifying underlying assumptions break down.

Here, we briefly consider the torque balance in a steady state system between the outward moving plasma and the $\mathbf{J} \times \mathbf{B}$ force from MI coupling, as shown in Figure 2. If we consider the ionosphere and the magnetosphere as two infinitely thin slabs, then the height-integrated current density, $\mathbf{K}$, rather than the current density, $\mathbf{J}$ is the relevant parameter. In an azimuthally symmetric system, the torque per unit length exerted on the system in the corotational direction from $\mathbf{J} \times \mathbf{B}$ forces is

$$\mathbf{T}_{j\times B} = \mathbf{r} \times (2\pi r \mathbf{K}_M \times \mathbf{B}_M) = 2\pi r^2 K_M B_M \hat{\theta} \tag{1}$$

where $\mathbf{T}_{j\times B}$ is the torque from $J\times B$ forces, $\mathbf{r}$ is the distance from the planetary spin axis, B_M is the magnetic field in the equatorial plane, and K_M is the magnetospheric height-integrated current density.

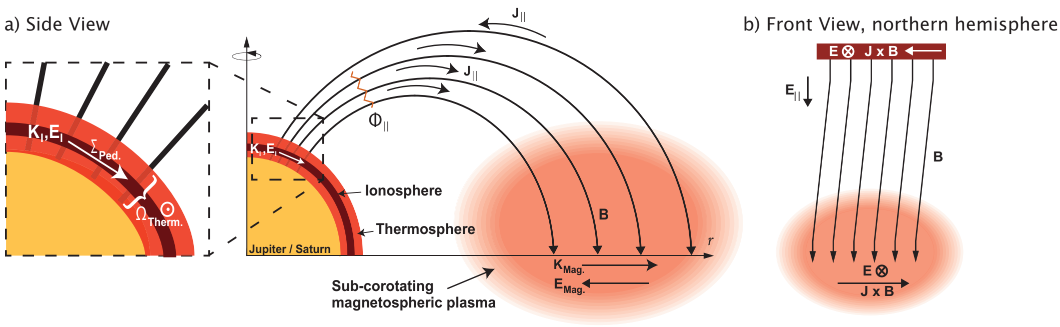

Figure 2. Geometry and associated fields for MI coupling in a system with internal plasma

The anti-corotational torque per unit length, $\mathbf{T}_M$, exerted on the plasma as it moves out through the system is

$$\mathbf{T}_M = \frac{d}{dr}\frac{d\mathbf{L}_M}{dt} = \dot{M}\frac{d}{dr}\mathbf{r}\times(\mathbf{r}\times\mathbf{\Omega}) = -\dot{M}\frac{d}{dr}r^2\Omega\hat{\theta} \tag{2}$$

where $\mathbf{L_M}$ is the angular momentum of the magnetospheric plasma, $\dot{M}$ is the radial mass transport rate in the magnetosphere, assumed to be constant throughout the system, and Ω is the plasma angular velocity, which is frame variant. Equation 2 can be modified to consider local pick-up processes by including a term to reflect the change in angular momentum from newly created plasma

$$\frac{d}{dr}\left(\dot{M}_{pu}r^2\left(\Omega_P - \Omega_N\right)\right) \tag{3}$$

where $\dot{M}_{pu}$ is the mass loading rate from ionization of neutrals, and Ω_P and Ω_N are the angular velocities of the planet and neutral material, respectively. As the system is in equilibrium, Equation 1, including the mass-loading term, and equation 2 must sum to zero, giving:

$$\dot{M}\frac{d}{dr}r^2\Omega + \frac{d}{dr}\left(\dot{M}_{pu}r^2\left(\Omega_P - \Omega_N\right)\right) = 2\pi r^2 K_M B_M \tag{4}$$

Equation 4 can be solved to determine latitudinal and radial profiles of the plasma angular velocity, ionospheric and magnetospheric electric fields, and currents within the MI coupled system. Ionospheric parameters can be related to their magnetospheric counterparts through current continuity, $\nabla\cdot\mathbf{J} = 0$, and conservation of magnetic flux. The magnetospheric height-integrated current density can be expressed as follows

$$K_M = -2K_I\frac{s}{r} = -2\Sigma_P E_I\frac{s}{r} \tag{5}$$

where K_I is the height-integrated ionospheric current density, Σ_P is the height-integrated Pedersen conductance, E_I is the ionospheric electric field, and s is the distance in the ionosphere from the spin axis. The factor of 2 reflects the northern and southern ionospheric contributions to the magnetospheric currents.

To consider non-idealized effects, one can numerically solve Equation 4 specifying radial profiles of magnetic field strength and mass-loading that reflect the system (e.g. Cowley & Bunce, 2001; D. H. Pontius & Hill, 2009; Ray et al., 2014; Saur et al., 2004). Feedback between the ionosphere and magnetosphere, which reflects changes in the atmosphere due to electron precipitation and joule heating, are included by modifying the

Pedersen conductance as a function of current density and/or electron precipitation energy (e.g. Nichols & Cowley, 2004; Ray et al., 2010; Ray, Ergun, et al., 2012). Real-time determination of the Pedersen conductance is computational prohibitive, so functional fits are based on detailed electron precipitation models, which investigate the ionospheric response to auroral precipitation (e.g. Galand, Moore, Mueller-Wodarg, Mendillo, & Miller, 2011; Millward, Miller, Stallard, Aylward, & Achilleos, 2002).

The persistant anti-corotational torque exerted in the ionosphere by $\mathbf{J} \times \mathbf{B}$ forces related to the extraction of angular momentum acts to slow the local thermosphere. Since the Pedersen conductivity depends on the ion-neutral collision frequency, which is a function of the relative velocity between the ions and neutrals, changes to the thermospheric angular velocity will modify the atmosphere's ability to conduct electrical current. These effects are discussed in more detail in Section 3. However, MI coupling models approximate the thermosphere-ionosphere interaction by defining an effective Pedersen conductance $\Sigma_P^* = (1-k)\Sigma_P$, first defined by Cowley, Bunce, and Nichols (2003):

$$k = \frac{\Omega_P - \Omega_P^*}{\Omega_P - \Omega} \tag{6}$$

where Ω_P^* is the angular velocity of the thermosphere, which is assumed to be intermediate between that of the planetary and plasma angular velocities.

Finally, the presence of high-latitude field-aligned electric potentials can modify how electric fields map between the ionosphere and magnetosphere. Any significant variation in the magnitude of field-aligned potentials with latitude must be considered through Faraday's Law, $\nabla \times \mathbf{E} = 0$, N.B. that we are ignoring $d\mathbf{B}/dt$ to consider a steady-state system. If this condition is met, then the magnetic field lines cannot be considered equipotentials and the electric fields between the ionosphere and magnetosphere are related by

$$E_I = \alpha \left(E_M - \frac{d\Phi_{||}}{dr} \right) \tag{7}$$

where $\Phi_{||}$ is the magnitude of the high-latitude field-aligned potentials. The mapping function, α, scales the electric fields using magnetic flux,

$$\alpha = B_I s / B_M r \tag{8}$$

where B_I and B_M are the magnitudes of the magnetic field at the ionosphere and magnetosphere, respectively. In order to numerically close the equations, the field-aligned potentials are related to the field-aligned current density via the Knight (1973) current-voltage relation.

$$J_{||} = j_x + j_x(R_x - 1)\left(1 - e^{-\frac{e\Phi_{||}}{T_x(R_x-1)}}\right) \tag{9}$$

where $j_x = en_x\sqrt{T_x/(2\pi m_E}$ is the electron thermal current density, e is the fundamental charge of an electron, R_x is the mirror ratio between the top of the acceleration region and the planet, and T_x is the energy of the electron source population. Ray et al. (2009) and Ray, Galand, Delamere, and Fleshman (2013) showed that the current-voltage relationship must be evaluated at the high-latitude location of the acceleration region in giant planet systems, typically between 2–3 planetary radii as measured from the center of the planet, because of the centrifugal confinement of magnetospheric plasma.

2.2 Breaking azimuthal symmetry

Most MI coupling models assume azimuthal symmetry; However, all planetary magnetospheres have intrinsic asymmetries introduced by the solar wind interaction. The extent to which these asymmetries penetrate into the magnetosphere and affect dynamics is a function of the planetary magnetic field strength and solar wind dynamic pressure. At Saturn, only the inner magnetosphere can be considered axisymmetric, while at Jupiter plasma flows are azimuthally symmetric within ∼30 R_J (Bagenal et al., 2016). However, statistical analysis of magnetic field data from Galileo indicates that asymmetries are present inside of 40 R_J (Vogt et al., 2011).

Azimuthal asymmetries can be captured by using MHD models or by applying MI coupling models to different local time sectors within the magnetosphere. There are advantages and disadvantages to each approach. The advantage of MHD models is that they capture the global behaviour of the magnetosphere, including solar wind disturbances and temporal changes (e.g. Chané et al., 2017; Jia, Hansen, et al., 2012; Walker & Ogino, 2003). They solve the continuity, momentum, and energy equations for ions and electrons. Mass loading and loss can be included via source and sink terms. Gravitational forces are explicitly included. Atmospheric effects can be approximated by including a term for ion-neutral collisions (Chané et al., 2013) or localized vortices at the inner boundary (Jia, Kivelson, & Gombosi, 2012). However, computational limitations prohibit the consideration of the high-latitude magnetosphere where the Alfvén velocity approaches the speed of light. To mitigate this effect, the inner boundary is set to a few planetary radii, restricting real-time feedback between the atmosphere and magnetosphere such as variations in the conductance with auroral precipitation.

The alternative to this approach is to apply MI coupling models at different local time slices within the magnetosphere (Ray et al., 2014). Each local time slice uses an appropriate equatorial magnetic field profile that reflects the asymmetries in the system. To date, only a constant ionospheric Pedersen conductance and equipotential field lines have been considered using this technique; However, including variations in the conductance and rotational decoupling between the ionosphere and magnetosphere should be the next step for static MI coupling models.

3 Atmospheric Theory

Magnetosphere-ionosphere coupling theory, as discussed so far, takes little account of the neutrals present within the thermosphere-ionosphere region of gas giant atmospheres. In this region, ions are influenced by electromagnetic forces but also by collisions with the neutrals in the ambient thermosphere. Let us first consider the simple case where ionospheric ions are acted on by electromagnetic forces only. The horizontal ion momentum equation, ignoring all but electromagnetic forces, is given by

$$m_i \dot{\mathbf{v}}_\mathbf{i} = \mathbf{e}\left(\mathbf{E} + \mathbf{v}_\mathbf{i} \times \mathbf{B}\right), \tag{10}$$

where $\dot{\mathbf{v}}_\mathbf{i}$ is the time derivative of the ion velocity $\mathbf{v}_\mathbf{i}$ in the inertial frame, and $\mathbf{E}$ and $\mathbf{B}$ are the electric and magnetic fields respectively. We can remove the electric field by switching to a reference frame that is moving at the plasma drift velocity ($\mathbf{v}_\mathbf{p}$) meaning that the ions and electrons forming the ionosphere's quasi-neutral plasma are at rest. Equation 10 now becomes

$$\dot{\mathbf{v}}'_\mathbf{i} = \mathbf{\Omega}_\mathbf{i} \mathbf{v}'_\mathbf{i} \times \hat{\mathbf{b}}. \tag{11}$$

The prime indicates that these quantities are in a reference frame that is moving at the plasma drift velocity, Ω_i is the ion gyrofrequency and $\hat{\mathbf{b}}$ is the magnetic field unit vector. This equation describes the average motion of the ions - circular motion perpendicular to the magnetic field combined with the plasma drift velocity. Ionospheric electrons behave similarly but rotate in the opposite direction to the ions.

In order to account for collisions between ionospheric ions and atmospheric neutrals an extra term, dependent on the ion-neutral collision frequency ν_{in} and the velocity difference between the two species, needs to be added to the momentum equation.

These ion-neutral collisions result in drag forces between the different atmospheric species modifying the momentum equation as follows

$$\dot{\mathbf{v}}_\mathbf{i}' = \mathbf{\Omega_i} \mathbf{v}_\mathbf{i}' \times \hat{\mathbf{b}} + \nu_{\mathbf{in}} \left(\mathbf{u}' - \mathbf{v}_\mathbf{i}' \right), \tag{12}$$

where $\mathbf{u}' = \mathbf{u} - \mathbf{v_p}$ and is the neutral bulk velocity in the plasma drift reference frame and $\mathbf{u}$ is the neutral velocity in the inertial frame. This collisional term represents momentum exchange between ions and neutrals and is called 'ion drag'.

Let us consider time scales which are long compared to the inverse of the ion gyrofrequency and ion-neutral collision frequency. One can then assume the system to be quasi-steady with zero net forces. Rearranging equation 12 for $\dot{\mathbf{v}}_\mathbf{i}$ and using the vector identity $\dot{\mathbf{v}}_\mathbf{i}' = -\left(\dot{\mathbf{v}}_\mathbf{i}' \times \hat{\mathbf{b}} \right) \times \hat{\mathbf{b}}$ gives the ion momentum equation in a form containing the neutral bulk velocity.

$$\dot{\mathbf{v}}_\mathbf{i}' = \mathbf{f}(\mathbf{r_i}) \mathbf{u}' \times \hat{\mathbf{b}} + \mathbf{r_i} \mathbf{f}(\mathbf{r_i}) \mathbf{u}', \tag{13}$$

where $f(r_i) = (r_i + r_i^{-1})^{-1}$ and $r_i = \nu_{in}/\Omega_i$. This equation gives the average ion velocity in the frame where we removed the electric field. If we also assume that electron-neutral collisions are negligible then in this frame, the ion velocity is in fact the relative velocity between ionospheric ions and electrons and will result in an 'ionic' current of current density $\mathbf{j} = |\mathbf{e}| \mathbf{n_i} \mathbf{v}_\mathbf{i}'$, where $|e|$ is the charge for a single-charged ion and n_i is the ion number density.

If we now switch to the neutral rest frame, the plasma drift velocity becomes $\mathbf{u}'$ which generates an electric field $\mathbf{E}^* = \mathbf{u}' \times \mathbf{B} = (\mathbf{u} - \mathbf{v_p}) \times \mathbf{B}$ and gives current density

$$\mathbf{j} = \sigma_\mathbf{P} \mathbf{E}^* + \sigma_\mathbf{H} \mathbf{E}^* \times \hat{\mathbf{b}}. \tag{14}$$

$\sigma_P = |e| n_i f(r_i) |B|^{-1}$ is the Pedersen conductivity and $\sigma_H = r_i \sigma_P$ is the Hall conductivity. From the conductivity relations one can see that the Pedersen conductivity maximizes at an altitude where $f(r_i = 1) = 0.5$ while the Hall conductivity maximises at low altitudes where $r_i f(r_i) = 1$. One therefore expects Pedersen currents (first term on the RHS of equation 14) to flow at higher altitudes than Hall currents (second term on the RHS of equation 14). Note that for multiple ion species the above current density and conductivities need to be summed over each species. These horizontal ionospheric currents close the field-aligned currents which connect the atmosphere-ionosphere system to a planet's magnetosphere and are responsible for the transfer of energy and angular momentum between the two regions.

The above description of the MIT current circuit is only a first order approximation. In reality, the atmosphere-ionosphere interacts with the magnetosphere not only by the quasi-steady large-scale currents discussed above but also by more complicated structures and dynamic phenomena. For example, magnetic field-aligned electric potentials accelerate plasma between planetary ionospheres and magnetospheres. Perpendicular spatial gradients in such structures decouple the plasma flows in the ionosphere and magnetosphere (e.g. Ray et al., 2015; Ray et al., 2009) (See section 2). A dynamic interaction between the ionosphere and magnetosphere results from Alfvén waves which carry field-aligned currents and stochastically accelerate plasma. We are only just realising the importance of this form of dynamic MIT coupling outside of moon-magnetosphere interactions because of in-situ measurements made by NASA's Juno mission (see section 4).

Returning to the simple circuit description. We can now represent the neutral momentum equation as

$$\frac{\partial \mathbf{u}}{\partial t} + (\mathbf{u}.\nabla)\,\mathbf{u} = \mathbf{f} + \mathbf{f_{ID}}, \tag{15}$$

where $\mathbf{f_{ID}} = \mathbf{j}\times\mathbf{B}$ and is the ion drag force per unit volume and $\mathbf{f}$ represents all other forces acting on the system.

At Jupiter and Saturn, assuming quasi-steady conditions, ion drag results in the acceleration of ionospheric ions towards corotation and the deceleration of neutrals. However, ion drag never stops the neutrals meaning that their momentum must be replenished and balanced somehow. Two mechanisms have been proposed which are capable of extracting angular momentum from the lower atmosphere and depositing it in the thermosphere-ionosphere region. These are i) vertical viscous transfer, and ii) meridional transfer from mid-to-high latitudes. Schematics showing these mechanisms are shown in Figs. 3a-b. Vertical viscous transfer of momentum at all latitudes (Fig. 3a) was proposed by Huang and Hill (1989) and D. H. Pontius (1995) to be the primary source of momentum transfer from the rigidly corotating lower atmosphere to the upper atmosphere. In this scenario, viscous processes supply a constant flow of momentum to the thermospheric neutrals which are being slowed down by the sub-corotating ions in the ionosphere. This is then transferred to the ions by the ion-neutral collisions and ultimately to the magnetospheric plasma via field-aligned currents. Recently, thermospheric general circulation models (GCMs) have shown vertical viscous transport from the lower atmosphere to be a relatively unimportant source of energy and momentum to gas giant thermospheres (e.g. Smith and Aylward (2008, 2009)). These atmospheric models showed that meridional transport from mid-to-high latitudes played a dominant role in transferring angular momentum from the lower atmosphere to the thermosphere (Fig. 3b). In this case, there is up-welling of neutrals and momentum from the lower atmosphere at mid-latitudes, which is transported polewards by meridional winds where momentum is exchanged before the neutrals down-well at the gas giant poles.

There are two energy sources associated with MI coupling and ion-neutral interactions. These are Joule heating and ion drag energy. Joule heating is heating due to electrical resistance - ohmic heating - but it can also be considered as a 'frictional heating' source due to friction between ions and neutrals. Ion drag energy is the change of kinetic energy associated with the ion drag force. The total energy associated with MI coupling Q_{tot} is given by equation 16. In MIT coupling models this total energy is mostly deposited in the Pedersen layer as shown in figure 3c.

$$Q_{tot} = \mathbf{j}\cdot\mathbf{E}^{*} + \mathbf{u}\cdot(\mathbf{j}\times\mathbf{B})\,. \tag{16}$$

4 Moving beyond steady-state in Giant Planet MIT coupling models

The gas giant planet magnetosphere-ionosphere coupling theory discussed above assumes that steady/quasi-steady conditions apply meaning that temporal variability in the magnetosphere and ionosphere, and the finite Alfvén travel time within the system are considered negligible. Such an assumption is usually acceptable when investigating the long-term averaged properties of the coupled system. In reality however, the system is never truly in a quasi-steady state - it is highly dynamic and not in force balance. Planetary magnetospheres are constantly being perturbed by time-dependent processes such as solar wind buffeting, magnetic reconnection and wave-particle interactions which in turn perturb the ionosphere and neutral thermosphere. The atmosphere, in return, further perturbs the magnetosphere as the system is coupled. It is clear that to truly understand the physics governing the coupled gas giant planet systems we need to consider the whole system under full time-dependence.

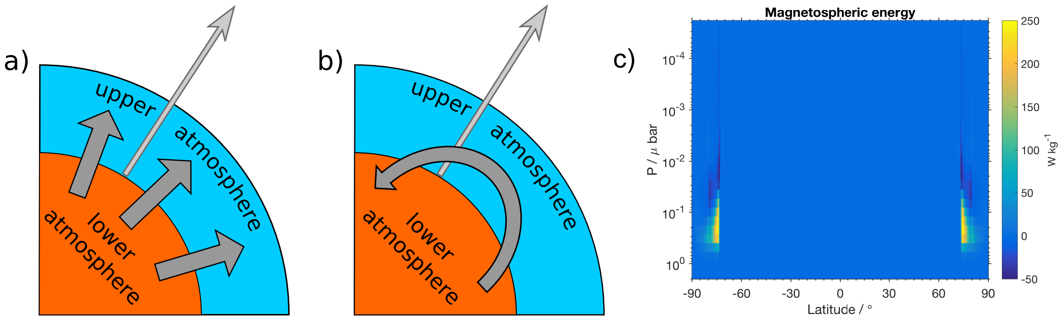

Figure 3. Schematic comparing viscous (a) and meridional transfer (b) of energy and momentum in gas giant atmospheres. Thick dark grey arrows show the direction of energy and momentum transport in the atmosphere while the thin light grey arrows indicate energy and momentum flow to the magnetosphere. Adapted from Smith and Aylward (2008). c) Deposition of magnetospheric energy (Joule heating and ion drag) within a 3D model thermosphere (based on Yates et al. (2012)) and assuming an axisymmetric magnetosphere model.

In the outer solar system, we typically have a single spacecraft in operation at any one time making it difficult to separate between spatial and temporal effects in observations. Numerical simulations are necessary to bridge the gap between single-point measurements and investigations of the time-dependent system on a global scale. However many numerical challenges exist in modeling either component of the coupled MIT system (some of which are discussed from the standpoint of global magnetospheric MHD models in chapter 11.1), let alone the system as a whole.

Time dependence is self-consistently included in all gas giant atmospheric general circulation models (GCMs). However, including time-dependence in the ionosphere-magnetosphere components of coupled MIT models is typical achieved through external forcing or detailed ionospheric chemistry (e.g. Achilleos et al., 1998). The latter requires long run times which can be prohibitive when considering feedback with the magnetosphere. In the former, the non-atmospheric portions of gas giant MIT models time-dependence has been included by varying the solar EUV flux (Tao et al., 2016) or the magnetopause radius (Yates et al., 2014; Yates et al., 2018). In these simulations, these quantities are changed over a portion of the simulation time and the resulting atmospheric response is investigated. Tao et al. (2016) found that by increasing the solar EUV flux at Jupiter by factors of two and three led to rapid (over a few planetary rotations) increases in mid-latitude thermospheric winds followed by a further delayed (tens of planetary rotations) response due to equatorward progpagation from the auroral zone and Joule heating. Yates et al. (2014) rapidly ($\leq$3 hours) varied the size of the magnetosphere to simulate solar wind compression and rarefaction regions. They found that both compressions and expansions result in an increase in atmospheric heating and brighter aurora but compressions also led to a change in north-south winds meaning that energy deposited in the auroral zone was transported equatorwards for the first time in a simulation.

The above proxies for including time-dependence in MIT coupling models are only a first step towards a true time-dependent MIT coupled model. One could also envisage the full coupling between a 3D atmospheric GCM, ionosphere model and a 3D magnetospheric MHD model. However, such a model setup is difficult to achieve due to the vastly different time-scales, and therefore spatial scales, required in order for the simulation to be self-consistent. Such models could include waves and their finite travel time but they could not self-consistently include include wave-particle interactions which have been found to play a vital role in gas giant MI coupling. In planetary magnetospheres information and field-aligned currents are carried by Alfvén waves and therefore any current system requires them in order to be established. The gas giant systems have been found to be rich with Alfvénic-type phenomena such as the satellite aurora resulting from the interaction of the Galilean satellites (at Jupiter) and Enceladus (at Saturn) with the gas giant magnetosphere (for a detailed description of jovian and kronian moon-planet interaction see chapter 9.3 by J. Saur and the references therein) to Alfvénic fluctuations (e.g Khurana & Kivelson, 1989; Kleindienst, Glassmeier, Simon, Dougherty, & Krupp, 2009; Mitchell et al., 2016; Yates et al., 2016) and particle acceleration (e.g Clark et al., 2018; Mauk et al., 2017a, 2017b; Saur et al., 2018).

Observations from NASA's Juno spacecraft have shown that the quasi-steady picture of jovian MIT coupling is far too simplistic to explain the observations. Juno found that auroral particle acceleration appears likely to arise from a combination of steady (inverted-V's and potential drops) and time-dependent (stochastic / wave-particle acceleration) processes as discussed in section 1.1. A new generation of numerical MIT coupling models is therefore necessary to explain the observations and gas giant MIT coupling. This new generation of models will not only need to take proper account of the neutral atmosphere but also the magnetosphere will need to be fully time-dependent and able to account for wave-particle interactions such as those discussed in Mauk and Saur (2007); Saur (2004); Saur et al. (2018). At Earth, numerical studies investigating time-dependent MIT coupling are extensive but typically focus on small-scale MIT coupling (e.g. Lysak, 1986; Yoshikawa, Amm, Vanhamki, & Fujii, 2011).

5 Model Results

We have a limited number of remote observations of gas giant atmospheres and fewer still in situ measurements, we therefore rely heavily on models to interpret the data we have and to understand the underlying physical processes occurring in these exotic systems. The last two decades have resulted in the development of a few gas giant MIT coupled models. These models all solve the atmosphere self-consistently but vary in their degree of accounting for the electromagnetic interaction with the magnetosphere. The models allow us to compare winds, composition, temperature, auroral emissions, heating rates and the conductivity of the thermosphere-ionosphere with available observations. Observed ionospheric winds of order 1 kms^{-1} (e.g. Johnson et al., 2017; Stallard et al., 2007) and auroral emissions (e.g. Clarke et al., 2009; Nichols, Clarke, Gérard, Grodent, & Hansen, 2009) are generally well reproduced by the suite of gas giant MIT coupling models.

Temperatures are a key model parameter and observable due to the giant planet *energy crisis* which highlights that the upper atmospheres of the solar system's giant planets are all at least twice as hot as one would expect if solar extreme ultraviolet (EUV) radiation was their main source of heat (e.g. Yelle & Miller, 2004). Heating from the magnetospheric interaction is thought to be key in heating the gas giant planets to their observed temperatures ($\sim$900 K for Jupiter and $\sim$400 K for Saturn). In the current models, the rapid gas giant rotation rates lead to most of this heat being trapped in the high-latitude polar regions while equatorial latitudes remain relatively cold at $\sim 200-300$ K. Some models get passed this issue by including other heat sources at mid- and low-latitudes such as heating due to gravity and/or acoustic wave breaking (currently poorly constrained due to the very limited in situ observations), modifying the ion drag and Joule heating rates, including extra Joule heating terms at low-latitudes, and/or including ad-hoc low-latitude heat sources. Despite models finding it difficult to reproduce low-latitude neutral temperatures, model temperatures in the polar regions are comparable to observations. Melin, Miller, Stallard, Smith, and Grodent (2006) analysed an auroral heating event observed by Stallard et al. (2001, 2002) thought to be caused by a magnetospheric expansion event. They found that, over a three day interval, integrated ion drag and Joule heating increased by $\sim$400%. Yates et al. (2014) used the Jupiter JASMIN MIT model to simulate how Jupiter's upper atmosphere responds to magnetospheric reconfigurations and found that a magnetospheric expansion resulted in a similar increase in integrated ion drag and Joule heating, albeit over a much shorter time scale (∼3 hours). These examples briefly highlight some of the benefits of complementing in situ spacecraft measurements and remote sensing observations with output from numerical simulations.

6 Conclusions

Magnetosphere-ionosphere-thermosphere coupling at the giant planets depends strongly on internal plasma sources and centrifugal forces from rapid rotation rates. Temporal variations in the outgassing rates of Io, at Jupiter, and Enceladus, at Saturn, combined with the non-steady nature of plasma transport throughout the system lead to dynamic systems with strong auroral emissions. Much of our understanding relies on in situ measurements from single spacecraft of plasma flows, magnetic fields, and precipitating particles, along with in situ and Earth-based remote observations. These observations help to guide our theoretical understanding of coupling between the atmosphere and the magnetosphere.

Juno and Cassini observations at high latitudes have recently revolutionized our understanding of MIT coupling within giant planet systems. Measurements of wave-driven particle acceleration requires that we revisit many of the underpinning assumptions used over the past four decades - namely that of quasi-static systems. Alfvénic processes are much more critical that previously thought. More work needs to be done to develop time-dependent models of MIT coupling that can fully consider the feedback between the atmosphere and magnetosphere.

References

Achilleos, N., Miller, S., Tennyson, J., Aylward, A. D., Mueller-Wodarg, I., & Rees, D. (1998, September). JIM: A time-dependent, three-dimensional model of Jupiter's thermosphere and ionosphere. *J. Geophys. Res.*, *103*, 20089-20112. doi: 10.1029/98JE00947

Allegrini, F., Bagenal, F., Bolton, S., Connerney, J., Clark, G., Ebert, R. W., ... Zink, J. L. (2017). Electron beams and loss cones in the auroral regions of jupiter. *Geophysical Research Letters*, *44*(14), 7131-7139. Retrieved from `https://agupubs.onlinelibrary.wiley.com/doi/abs/10.1002/2017GL073180` doi: 10.1002/2017GL073180

Atreya, S. K., Donahue, T. M., Sandel, B. R., Broadfoot, A. L., & Smith, G. R. (1979). Jovian upper atmospheric temperature measurement by the voyager 1 uv spectrometer. *Geophysical Research Letters*, *6*(10), 795-798. Retrieved from `https://agupubs.onlinelibrary.wiley.com/doi/abs/10.1029/GL006i010p00795` doi: 10.1029/GL006i010p00795

Badman, S. V., Cowley, S. W. H., Gérard, J.-C., & Grodent, D. (2006, December). A statistical analysis of the location and width of Saturn's southern auroras. *Annales Geophysicae*, *24*, 3533-3545. doi: 10.5194/angeo-24-3533-2006

Badman, S. V., Cowley, S. W. H., Lamy, L., Cecconi, B., & Zarka, P. (2008). Relationship between solar wind corotating interaction regions and the phasing and intensity of saturn kilometric radiation bursts. *Annales Geophysicae*, *26*(12), 3641–3651. Retrieved from `https://www.ann-geophys.net/26/3641/2008/` doi: 10.5194/angeo-26-3641-2008

Bagenal, F., Wilson, R. J., Siler, S., Paterson, W. R., & Kurth, W. S. (2016, May). Survey of Galileo plasma observations in Jupiter's plasma sheet. *Journal of Geophysical Research (Planets)*, *121*, 871-894. doi: 10.1002/2016JE005009

Branduardi-Raymont, G., Elsner, R. F., Galand, M., Grodent, D., Cravens, T. E., Ford, P., ... Waite, J. H. (2008, February). Spectral morphology of the X-ray emission from Jupiter's aurorae. *Journal of Geophysical Research (Space Physics)*, *113*, 2202. doi: 10.1029/2007JA012600

Chané, E., Saur, J., Keppens, R., & Poedts, S. (2017). How is the jovian main auroral emission affected by the solar wind? *Journal of Geophysical Research: Space Physics*, *122*(2), 1960-1978. Retrieved from https://agupubs.onlinelibrary.wiley.com/doi/abs/10.1002/2016JA023318 doi: 10.1002/2016JA023318

Chané, E., Saur, J., & Poedts, S. (2013, May). Modeling Jupiter's magnetosphere: Influence of the internal sources. *J. Geophys. Res.*, *118*, 2157-2172. doi: 10.1002/jgra.50258

Clark, G., Tao, C., Mauk, B. H., Nichols, J., Saur, J., Bunce, E. J., ... Valek, P. (2018). Precipitating electron energy flux and characteristic energies in jupiter's main auroral region as measured by juno/jedi. *Journal of Geophysical Research: Space Physics*, *0*(ja). Retrieved from https://agupubs.onlinelibrary.wiley.com/doi/abs/10.1029/2018JA025639 doi: 10.1029/2018JA025639

Clarke, J. T., Grodent, D., Cowley, S. W. H., Bunce, E. J., Zarka, P., Connerney, J. E. P., & Satoh, T. (2004). Jupiter's aurora. In (p. 639-670). Jupiter. The Planet, Satellites and Magnetosphere.

Clarke, J. T., Nichols, J., Gérard, J., Grodent, D., Hansen, K. C., Kurth, W., ... Cecconi, B. (2009, May). Response of Jupiter's and Saturn's auroral activity to the solar wind. *J. Geophys. Res.*, *114*, A05210. doi: 10.1029/2008JA013694

Cowley, S. W. H., & Bunce, E. J. (2001, August). Origin of the main auroral oval in Jupiter's coupled magnetosphere-ionosphere system. *Planetary and Space Science*, *49*, 1067-1088.

Cowley, S. W. H., Bunce, E. J., & Nichols, J. D. (2003, January). Origins of Jupiter's main oval auroral emissions. *J. Geophys. Res.*, *108*. doi: 10.1029/2002JA009329

Delamere, P. A., Bagenal, F., & Steffl, A. (2005, December). Radial variations in the Io plasma torus during the Cassini era. *J. Geophys. Res.*, *110*. doi: 10.1029/2005JA011251

Drossart, P., Maillard, J.-P., Caldwell, J., Kim, S. J., Watson, J. K. G., Majewski, W. A., ... Wagener, R. (1989, August). Detection of H3(+) on Jupiter. *Nature*, *340*, 539-541. doi: 10.1038/340539a0

Dunn, W. R., Branduardi-Raymont, G., Ray, L. C., Jackman, C. M., Kraft, R. P., Elsner, R. F., ... Coates, A. J. (2017, November). The independent pulsations of Jupiter's northern and southern X-ray auroras. *Nature Astronomy*, *1*, 758-764. doi: 10.1038/s41550-017-0262-6

Ergun, R. E., Carlson, C. W., McFadden, J. P., Delory, G. T., Strangeway, R. J., & Pritchett, P. L. (2000, July). Electron-Cyclotron Maser Driven by Charged-Particle Acceleration from Magnetic Field-aligned Electric Fields. *The Astrophysical Journal*, *538*, 456-466.

Galand, M., Moore, L., Mueller-Wodarg, I., Mendillo, M., & Miller, S. (2011, September). Response of Saturn's auroral ionosphere to electron precipitation: Electron density, electron temperature, and electrical conductivity. *J. Geophys. Res.*, *116*, A09306. doi: 10.1029/2010JA016412

Hansen, C. J., Esposito, L., Stewart, A. I. F., Colwell, J., Hendrix, A., Pryor, W., ... West, R. (2006, March). Enceladus' Water Vapor Plume. *Science*, *311*, 1422-1425. doi: 10.1126/science.1121254

Hess, S. L. G., Delamere, P., Dols, V., Bonfond, B., & Swift, D. (2010, June). Power transmission and particle acceleration along the Io flux tube. *J. Geophys. Res.*, *115*, A06205. doi: 10.1029/2009JA014928

Hess, S. L. G., & Delamere, P. A. (2012). Satellite-induced electron acceleration and related auroras. In A. Keiling, E. Donovan, F. Bagenal, & T. Karlsson

(Eds.), *Auroral phenomenology and magnetospheric processes: Earth and other planets.* American Geophysical Union. doi: 10.1029/2011GM001175

Hill, T. W. (1979, November). Inertial limit on corotation. *J. Geophys. Res.*, *84*, 6554-6558.

Huang, T. S., & Hill, T. W. (1989, April). Corotation lag of the Jovian atmosphere, ionosphere, and magnetosphere. *J. Geophys. Res.*, *94*, 3761-3765.

Hunt, G. J., Provan, G., Bunce, E. J., Cowley, S. W. H., Dougherty, M. K., & Southwood, D. J. (2018, May). Field-Aligned Currents in Saturn's Magnetosphere: Observations From the F-Ring Orbits. *Journal of Geophysical Research (Space Physics)*, *123*, 3806-3821. doi: 10.1029/2017JA025067

Jacobsen, S., Neubauer, F. M., Saur, J., & Schilling, N. (2007). Io's nonlinear mhd-wave field in the heterogeneous jovian magnetosphere. *Geophysical Research Letters*, *34*(10). doi: 10.1029/2006GL029187

Jia, X., Hansen, K. C., Gombosi, T. I., Kivelson, M. G., Tth, G., DeZeeuw, D. L., & Ridley, A. J. (2012). Magnetospheric configuration and dynamics of saturn's magnetosphere: A global mhd simulation. *Journal of Geophysical Research: Space Physics*, *117*(A5). Retrieved from `https://agupubs.onlinelibrary.wiley.com/doi/abs/10.1029/2012JA017575` doi: 10.1029/2012JA017575

Jia, X., Kivelson, M. G., & Gombosi, T. I. (2012). Driving saturn's magnetospheric periodicities from the upper atmosphere/ionosphere. *Journal of Geophysical Research: Space Physics*, *117*(A4). Retrieved from `https://agupubs.onlinelibrary.wiley.com/doi/abs/10.1029/2011JA017367` doi: 10.1029/2011JA017367

Johnson, R. E., Stallard, T. S., Melin, H., Nichols, J. D., & Cowley, S. W. H. (2017, July). Jupiter's polar ionospheric flows: High resolution mapping of spectral intensity and line-of-sight velocity of H_3^+ ions. *Journal of Geophysical Research (Space Physics)*, *122*, 7599-7618. doi: 10.1002/2017JA024176

Khurana, K. K. (2001, November). Influence of solar wind on Jupiter's magnetosphere deduced from currents in the equatorial plane. *J. Geophys. Res.*, *106*, 25999-26016. doi: 10.1029/2000JA000352

Khurana, K. K., & Kivelson, M. G. (1989, May). Ultralow frequency MHD waves in Jupiter's middle magnetosphere. *Journal of Geophysical Research*, *94*, 5241-5254. doi: 10.1029/JA094iA05p05241

Kleindienst, G., Glassmeier, K.-H., Simon, S., Dougherty, M. K., & Krupp, N. (2009, February). Quasiperiodic ULF-pulsations in Saturn's magnetosphere. *Annales Geophysicae*, *27*, 885-894. doi: 10.5194/angeo-27-885-2009

Knight, S. (1973, May). Parallel electric fields. *Planetary and Space Science*, *21*, 741-750.

Kurth, W. S., Imai, M., Hospodarsky, G. B., Gurnett, D. A., Louarn, P., Valek, P., ... Zarka, P. (2017). A new view of jupiter's auroral radio spectrum. *Geophysical Research Letters*, *44*(14), 7114-7121. doi: 10.1002/2017GL072889

Kurth, W. S., Mauk, B. H., Elliott, S. S., Gurnett, D. A., Hospodarsky, G. B., Santolik, O., ... Levin, S. M. (2018). Whistler mode waves associated with broadband auroral electron precipitation at jupiter. *Geophysical Research Letters*, *45*(18), 9372-9379. doi: 10.1029/2018GL078566

Lam, H. A., Achilleos, N., Miller, S., Tennyson, J., Trafton, L. M., Geballe, T. R., & Ballester, G. E. (1997, June). A Baseline Spectroscopic Study of the Infrared Auroras of Jupiter. *Icarus*, *127*, 379-393. doi: 10.1006/icar.1997.5698

Lamy, L., Prangé, R., Pryor, W., Gustin, J., Badman, S. V., Melin, H., ... Brandt, P. C. (2013). Multispectral simultaneous diagnosis of saturn's aurorae throughout a planetary rotation. *Journal of Geophysical Research: Space Physics*, *118*(8), 4817-4843. Retrieved from `https://agupubs.onlinelibrary.wiley.com/doi/abs/10.1002/jgra.50404` doi: 10.1002/jgra.50404

Lamy, L., Zarka, P., Cecconi, B., Prangé, R., Kurth, W. S., Hospodarsky, G., ...

Hunt, G. J. (2018). The low-frequency source of saturn's kilometric radiation. *Science*, *362*(6410). Retrieved from https://science.sciencemag.org/content/362/6410/eaat2027 doi: 10.1126/science.aat2027

Lysak, R. L. (1986). Coupling of the dynamic ionosphere to auroral flux tubes. *Journal of Geophysical Research: Space Physics*, *91*(A6), 7047-7056. Retrieved from https://agupubs.onlinelibrary.wiley.com/doi/abs/10.1029/JA091iA06p07047 doi: 10.1029/JA091iA06p07047

Matsuda, K., Terada, N., Katoh, Y., & Misawa, H. (2012, October). A simulation study of the current-voltage relationship of the Io tail aurora. *Journal of Geophysical Research (Space Physics)*, *117*, 10214. doi: 10.1029/2012JA017790

Mauk, B. H., Haggerty, D. K., Paranicas, C., Clark, G., Kollmann, P., Rymer, A. M., ... Valek, P. (2017a, 09 06). Discrete and broadband electron acceleration in jupiter's powerful aurora. *Nature*, *549*, 66 EP -. Retrieved from http://dx.doi.org/10.1038/nature23648

Mauk, B. H., Haggerty, D. K., Paranicas, C., Clark, G., Kollmann, P., Rymer, A. M., ... Valek, P. (2017b). Diverse electron and ion acceleration characteristics observed over jupiter's main aurora. *Geophysical Research Letters*, *45*(3), 1277-1285. Retrieved from https://agupubs.onlinelibrary.wiley.com/doi/abs/10.1002/2017GL076901 doi: 10.1002/2017GL076901

Mauk, B. H., & Saur, J. (2007, October). Equatorial electron beams and auroral structuring at Jupiter. *J. Geophys. Res.*, *112*. doi: 10.1029/2007JA012370

McNutt, R. L., Jr., Belcher, J. W., Sullivan, J. D., Bagenal, F., & Bridge, H. S. (1979, August). Departure from rigid co-rotation of plasma in Jupiter's dayside magnetosphere. *Nature*, *280*, 803.

Melin, H., Miller, S., Stallard, T., Smith, C., & Grodent, D. (2006, March). Estimated energy balance in the jovian upper atmosphere during an auroral heating event. *Icarus*, *181*, 256-265. doi: 10.1016/j.icarus.2005.11.004

Melrose, D. B., & Dulk, G. A. (1982, August). Electron-cyclotron masers as the source of certain solar and stellar radio bursts. *The Astrophysical Journal*, *259*, 844-858. doi: 10.1086/160219

Millward, G., Miller, S., Stallard, T., Aylward, A. D., & Achilleos, N. (2002, November). On the Dynamics of the Jovian Ionosphere and Thermosphere III. The Modelling of Auroral Conductivity. *Icarus*, *160*, 95-107. doi: 10.1006/icar.2002.6951

Mitchell, D. G., Carbary, J. F., Bunce, E. J., Radioti, A., Badman, S. V., Pryor, W. R., ... Kurth, W. S. (2016, January). Recurrent pulsations in Saturn's high latitude magnetosphere. *Icarus*, *263*, 94-100. doi: 10.1016/j.icarus.2014.10.028

Mitchell, D. G., Kurth, W. S., Hospodarsky, G. B., Krupp, N., Saur, J., Mauk, B. H., ... Hamilton, D. C. (2009). Ion conics and electron beams associated with auroral processes on saturn. *Journal of Geophysical Research: Space Physics*, *114*(A2). Retrieved from https://agupubs.onlinelibrary.wiley.com/doi/abs/10.1029/2008JA013621 doi: 10.1029/2008JA013621

Mueller-Wodarg, I. M. (2012). STIM GCM. *Icarus*, *25*, 1629-1632. doi: 10.1029/98GL00849

Nichols, J. D., Clarke, J. T., Gérard, J. C., Grodent, D., & Hansen, K. C. (2009, June). Variation of different components of Jupiter's auroral emission. *J. Geophys. Res.*, *114*. doi: 10.1029/2009JA014051

Nichols, J. D., & Cowley, S. W. H. (2004, May). Magnetosphere-ionosphere coupling currents in Jupiter's middle magnetosphere: effect of precipitation-induced enhancement of the ionospheric Pedersen conductivity. *Ann. Geophys.*, *22*, 1799-1827. doi: 10.5194/angeo-22-1799-2004

Nichols, J. D., & Cowley, S. W. H. (2005, March). Magnetosphere-ionosphere coupling currents in Jupiter's middle magnetosphere: effect of magnetosphere-ionosphere decoupling by field-aligned auroral voltages. *Ann. Geophys.*, *23*,

799-808.
Pontius, D. H. (1995, October). Implications of variable mass loading in the Io torus: The Jovian flywheel. *J. Geophys. Res*, *100*, 19531-19540. doi: 10.1029/95JA01554
Pontius, D. H. (1997, April). Radial mass transport and rotational dynamics. *J. Geophys. Res.*, *102*, 7137-7150. doi: 10.1029/97JA00289
Pontius, D. H., & Hill, T. W. (2009, December). Plasma mass loading from the extended neutral gas torus of Enceladus as inferred from the observed plasma corotation lag. *Geophys. Res. Letters*, *36*, 23103. doi: 10.1029/2009GL041030
Pontius, D. H., Jr., & Hill, T. W. (1982, December). Departure from corotation of the Io plasma torus - Local plasma production. *Geophys. Res. Lett.*, *9*, 1321-1324.
Ray, L. C., Achilleos, N. A., Vogt, M. F., & Yates, J. N. (2014, June). Local time variations in Jupiter's magnetosphere-ionosphere coupling system. *Journal of Geophysical Research (Space Physics)*, *119*, 4740-4751. doi: 10.1002/2014JA019941
Ray, L. C., Achilleos, N. A., & Yates, J. N. (2015). The effect of including field-aligned potentials in the coupling between jupiter's thermosphere, ionosphere, and magnetosphere. *Journal of Geophysical Research: Space Physics*, *120*(8), 6987-7005. doi: 10.1002/2015JA021319
Ray, L. C., Ergun, R. E., Delamere, P. A., & Bagenal, F. (2010, September). Magnetosphere-ionosphere coupling at Jupiter: Effect of field-aligned potentials on angular momentum transport. *J. Geophys. Res.*, *115*, A09211. doi: 10.1029/2010JA015423
Ray, L. C., Ergun, R. E., Delamere, P. A., & Bagenal, F. (2012, January). Magnetosphere-ionosphere coupling at Jupiter: A parameter space study. *J. Geophys. Res.*, *117*, A01205. doi: 10.1029/2011JA016899
Ray, L. C., Galand, M., Delamere, P. A., & Fleshman, B. L. (2013, June). Current-voltage relation for the Saturnian system. *Journal of Geophysical Research (Space Physics)*, *118*, 3214-3222. doi: 10.1002/jgra.50330
Ray, L. C., Galand, M., Moore, L. E., & Fleshman, B. L. (2012, July). Characterizing the limitations to the coupling between Saturn's ionosphere and middle magnetosphere. *Journal of Geophysical Research (Space Physics)*, *117*, 7210. doi: 10.1029/2012JA017735
Ray, L. C., Su, Y., Ergun, R. E., Delamere, P. A., & Bagenal, F. (2009, April). Current-voltage relation of a centrifugally confined plasma. *J. Geophys. Res.*, *114*. doi: 10.1029/2008JA013969
Saur, J. (2004, January). A model of Io's local electric field for a combined Alfvénic and unipolar inductor far-field coupling. *J. Geophys. Res.*, *109*. doi: 10.1029/2002JA009354
Saur, J., Janser, S., Schreiner, A., Clark, G., Mauk, B. H., Kollmann, P., . . . Kotsiaros, S. (2018). Wave-particle interaction of alfvn waves in jupiter's magnetosphere: Auroral and magnetospheric particle acceleration. *Journal of Geophysical Research: Space Physics*. doi: 10.1029/2018JA025948
Saur, J., Mauk, B. H., Kaßner, A., & Neubauer, F. M. (2004, May). A model for the azimuthal plasma velocity in Saturn's magnetosphere. *J. Geophys. Res.*, *109*, 5217. doi: 10.1029/2003JA010207
Smith, C. G. A., & Aylward, A. D. (2008, May). Coupled rotational dynamics of Saturn's thermosphere and magnetosphere: a thermospheric modelling study. *Annales Geophysicae*, *26*, 1007-1027. doi: 10.5194/angeo-26-1007-2008
Smith, C. G. A., & Aylward, A. D. (2009, January). Coupled rotational dynamics of Jupiter's thermosphere and magnetosphere. *Annales Geophysicae*, *27*, 199-230.
Stallard, T., Miller, S., Melin, H., Lystrup, M., Dougherty, M., & Achilleos, N. (2007, July). Saturn's auroral/polar H_3^+ infrared emission. I. Gen-

eral morphology and ion velocity structure. *Icarus*, *189*, 1-13. doi: 10.1016/j.icarus.2006.12.027

Stallard, T., Miller, S., Millward, G., & Joseph, R. D. (2001, December). On the Dynamics of the Jovian Ionosphere and Thermosphere. I. The Measurement of Ion Winds. *Icarus*, *154*, 475-491. doi: 10.1006/icar.2001.6681

Stallard, T., Miller, S., Millward, G., & Joseph, R. D. (2002, April). On the Dynamics of the Jovian Ionosphere and Thermosphere. II. The Measurement of H_3^+ Vibrational Temperature, Column Density, and Total Emission. *Icarus*, *156*, 498-514. doi: 10.1006/icar.2001.6793

Su, Y., Ergun, R. E., Bagenal, F., & Delamere, P. A. (2003, February). Io-related Jovian auroral arcs: Modeling parallel electric fields. *J. Geophys. Res.*, *108*. doi: 10.1029/2002JA009247

Su, Y.-J., Jones, S. T., Ergun, R. E., Bagenal, F., Parker, S. E., Delamere, P. A., & Lysak, R. L. (2006). Io-jupiter interaction: Alfvn wave propagation and ionospheric alfvn resonator. *Journal of Geophysical Research: Space Physics*, *111*(A6). doi: 10.1029/2005JA011252

Talboys, D. L., Arridge, C. S., Bunce, E. J., Coates, A. J., Cowley, S. W. H., & Dougherty, M. K. (2009, June). Characterization of auroral current systems in Saturn's magnetosphere: High-latitude Cassini observations. *J. Geophys. Res.*, *114*. doi: 10.1029/2008JA013846

Tao, C., Kimura, T., Badman, S. V., André, N., Tsuchiya, F., Murakami, G., ... Fujimoto, M. (2016, May). Variation of Jupiter's aurora observed by Hisaki/EXCEED: 2. Estimations of auroral parameters and magnetospheric dynamics. *Journal of Geophysical Research (Space Physics)*, *121*, 4055-4071. doi: 10.1002/2015JA021272

Thomsen, M. F., Reisenfeld, D. B., Delapp, D. M., Tokar, R. L., Young, D. T., Crary, F. J., ... Williams, J. D. (2010, October). Survey of ion plasma parameters in Saturn's magnetosphere. *J. Geophys. Res.*, *115*, 10220. doi: 10.1029/2010JA015267

Vogt, M. F., Kivelson, M. G., Khurana, K. K., Walker, R. J., Bonfond, B., Grodent, D., & Radioti, A. (2011, March). Improved mapping of Jupiter's auroral features to magnetospheric sources. *J. Geophys. Res.*, *116*, 3220. doi: 10.1029/2010JA016148

Walker, R. J., & Ogino, T. (2003, April). A simulation study of currents in the Jovian magnetosphere. *Planetary and Space Science*, *51*, 295-307. doi: 10.1016/S0032-0633(03)00018-7

Wu, C. S., & Lee, L. C. (1979, June). A theory of the terrestrial kilometric radiation. *The Astrophysical Journal*, *230*, 621-626. doi: 10.1086/157120

Yates, J. N., Achilleos, N., & Guio, P. (2012, February). Influence of upstream solar wind on thermospheric flows at Jupiter. *Planetary and Space Science*, *61*, 15-31. doi: 10.1016/j.pss.2011.08.007

Yates, J. N., Achilleos, N., & Guio, P. (2014, February). Response of the Jovian thermosphere to a transient pulse in solar wind pressure. *Planetary and Space Science*, *91*, 27-44. doi: 10.1016/j.pss.2013.11.009

Yates, J. N., Ray, L. C., & Achilleos, N. (2018). An initial study into the long-term influence of solar wind dynamic pressure on jupiter's thermosphere. *Journal of Geophysical Research: Space Physics*. Retrieved from `https://agupubs.onlinelibrary.wiley.com/doi/abs/10.1029/2018JA025828` doi: 10.1029/2018JA025828

Yates, J. N., Southwood, D. J., Dougherty, M. K., Sulaiman, A. H., Masters, A., Cowley, S. W. H., ... Coates, A. J. (2016, November). Saturn's quasiperiodic magnetohydrodynamic waves. *Geophysical Research Letters*, *43*, 11. doi: 10.1002/2016GL071069

Yelle, R. V., & Miller, S. (2004). Jupiter's thermosphere and ionosphere. In F. Bagenal, T. E. Dowling, & W. B. McKinnon (Eds.), *Jupiter. the planet, satellites*

and magnetosphere (p. 185-218).
Yoshikawa, A., Amm, O., Vanhamki, H., & Fujii, R. (2011). A self-consistent synthesis description of magnetosphere-ionosphere coupling and scale-dependent auroral process using shear alfvn wave. *Journal of Geophysical Research: Space Physics*, *116*(A8). Retrieved from https://agupubs.onlinelibrary.wiley.com/doi/abs/10.1029/2011JA016460 doi: 10.1029/2011JA016460
Zarka, P. (1998). Auroral radio emissions at the outer planets: Observations and theories. *Journal of Geophysical Research: Planets*, *103*(E9), 20159-20194. doi: 10.1029/98JE01323